Supporting Information

He and Bjorkman 10.1073/pnas.1106925108

SI Materials and Methods

CryoEM Data Collection and Reconstruction. A total of ~2 μL of purified FcRY (~3.0 mg/mL in pH 6.0 or pH 8.0 buffer) was loaded onto glow-discharged lacey carbon grids (Ted Pella, Inc.) and vitrified in liquid nitrogen using an FEI vitrobot. Frozen grids were transferred to an FEI Tecnai G2 Polara microscope for imaging on a 4k × 4k charge-coupled device with a nominal magnification of 50,000 at a dose of ~$20e^{-}/A^{2}$. Imaging was performed at 300 kV at defocus values of 2–5 μm. The exact image defocus was later determined by CTFFIND3 (1). The program EMAN (2) was used for particle selection and initial model building. Frealign (3) was used for orientation refinement and 3D reconstructions, and Chimera (4) was used for density display. The approximate resolution of the reconstruction was determined with a 0.5 Fourier shell correlation cutoff calculated using Frealign.

The images of FcRY at pH 6.0 showed a mixture of monomeric and, more rarely, dimeric FcRY, correlating with previous reports that the FcRY ectodomain can dimerize at high protein concentrations (5). A total of 11,745 particles were selected for reconstruction of the FcRY monomer, and 1,883 particles for the dimer. The initial reconstruction of the FcRY monomer was generated using the program startAny of EMAN (2) without symmetry averaging. Electron density was calculated to 25 Å resolution from high-resolution crystal structures of proteins homologous to FcRY domains (Fig. 1*B*; PDB codes 1DQO, 2FN2, and 2CL8 for CysR, FNII, and the CTLD domains, respectively), and the densities were docked into the EM density manually using the program Chimera (4). Individual domains were assigned to locations within high contour-level FcRY density using the knowledge of the order of the domains in the FcRY ectodomain. A reconstruction for the FcRY dimer structure was generated independently following a procedure similar to that used for the monomer at pH 6, but including twofold symmetry averaging using an initial model built by the program startcsym within EMAN (2). Two copies of the domain assignment generated for the FcRY monomer structure were found to fit the density generated for the dimer reconstruction. A reconstruction from 1,829 particles of FcRY at pH 8 was attempted without success, presumably due to flexibility of the FcRY ectodomain at basic pH.

FcRY–FcY and FcRY–IgY complexes were prepared at pH 6.0 by mixing FcRY with FcY or IgY at a 2:1 molar ratio. Complexes were loaded onto grids at concentrations between 3 and 4 mg/mL. A total of 3,835 particles and 4,572 particles were selected for FcRY–FcY and FcRY–IgY complexes, respectively. Data collection and reconstructions were done as described previously. The structures were examined independently and then combined to reconstruct an FcRY–IgY structure from 8,407 total particles. Twofold symmetry was used for as described for the FcRY dimer in model building and refinement. Electron density from the FcY structure (PDB code 2W59) was generated to 25 Å resolution, and the FcRY monomer structure and FcY density were fit into the FcRY–IgY complex density as described previously. The handedness of the FcRY–IgY complex density map was determined based on the handedness of the FcY structure. The fitting of density for the FcRY monomer structure into the complex density map then determined the handedness of the FcRY monomer and dimer.

SAXS Data Collection and Analysis. SAXS data were collected at beamline 4-2 at the Stanford Synchrotron Radiation Lightsource as described (6). Samples (30 μL of FcRY at pH 6.0 or 8.0) were loaded into tubes on a loading block for automatic sample feeding. All samples had been previously passed over a Superdex 200 gel filtration column to remove potential aggregates. A series of 10 measurements were recorded on a MarCCD detector with exposure times of 2 s for each sample and its corresponding buffer solution. The samples were kept at 15 °C during the exposures. Data were collected from a concentration series of FcRY (0.25–5.0 mg/mL) at pH 6.0 and pH 8.0 to evaluate potential concentration-dependent effects.

Scattering data were analyzed using the ATSAS program suite (7). The program Primus (8) was used to calculate a Guinier plot to determine values for the radius of gyration, R_g, using a 1.3 cutoff for sRg. The linearity of the Guinier plots suggested that the samples were monodisperse. The pair distribution function was calculated by the program GNOM (9), and the low-resolution envelopes for FcRY at pH 6 and pH 8 were calculated using the program GASBOR (10).

FcRY Mutagenesis. FcRY histidine mutants (H159Y, H387Q, H538Q, H962Y, and H978S) were prepared from the wild-type gene using a QuikChange Site-Directed Mutagenesis Kit (Stratagene), and the altered genes were subcloned into the mammalian expression vector pcDNA3.1 (Invitrogen). Mutant proteins and wild-type FcRY were transiently expressed in HEK293 cells. The proteins were purified and exchanged into pH 6.0 and 8.0 buffers as described for wild-type FcRY expressed in insect cells. The migrations of the mutant proteins were compared with wild-type FcRY by gel filtration chromatography using a Superdex 200 (16/60) column run at pH 6 and pH 8.

SI Results and Discussion

The mechanism by which the FcRY structure changes with pH could involve titration of histidines, which have a pK_a within the narrow range near the neutral pH of the FcRY conformational change. Based on the domain arrangement deduced from the cryoEM reconstruction of FcRY at pH 6 (Fig. 2), we identified five histidines that are conserved between chicken and finch FcRY sequences and are located in domains likely to be involved in the pH-dependent conformational change (FNII, CTLD2, and CTLD6). We altered these by site-directed mutagenesis to create five single-site FcRY mutants: H159Y, H387Q, H538Q, H962Y, and H978S. In each case, the histidine residue was substituted to its corresponding residue in mammalian PLA_2R, the closest relative of FcRY in the MR family (5). Purified FcRY mutants were examined by size exclusion chromatography at pH 6 and 8. Each mutant showed changes in migration as a function of pH, as seen for wild-type FcRY (Fig. S4), thus none of the targeted histidines in isolation was responsible for the pH-dependent conformational change.

1. Mindell JA, Grigorieff N (2003) Accurate determination of local defocus and specimen tilt in electron microscopy. *J Struct Biol* 142:334–347.
2. Ludtke SJ, Baldwin PR, Chiu W (1999) EMAN: Semiautomated software for high-resolution single-particle reconstructions. *J Struct Biol* 128:82–97.
3. Grigorieff N (2007) FREALIGN: High-resolution refinement of single particle structures. *J Struct Biol* 157:117–125.
4. Goddard TD, Huang CC, Ferrin TE (2007) Visualizing density maps with UCSF Chimera. *J Struct Biol* 157:281–287.

5. West AP, Jr., Herr AB, Bjorkman PJ (2004) The chicken yolk sac IgY receptor, a functional equivalent of the mammalian MHC-related Fc receptor, is a phospholipase A2 receptor homolog. *Immunity* 20:601–610.
6. Smolsky IL, et al. (2007) Biological small-angle X-ray scatterig facility at the Stanford Synchrotron Radiation Laboratory. *J Appl Cryst* 40:s453–s458.
7. Konarev PV, Petoukhov MV, Volkov VV, Svergun DI (2006) ATSAS 2.1, a program package for small-angle scattering data analysis. *J Appl Cryst* 39:277–286.
8. Konarev PV, Volkov VV, Sokolova AV, Koch MHJ, Svergun DI (2003) PRIMUS: A Windows PC-based system for small-angle scattering data analysis. *J Appl Cryst* 36: 1277–1282.
9. Svergun D (1992) Determination of the regularization parameter in indirect-transform methods using perceptual criteria. *J Appl Cryst* 25:495–503.
10. Svergun DI, Petoukhov MV, Koch MH (2001) Determination of domain structure of proteins from X-ray solution scattering. *Biophys J* 80:2946–2953.

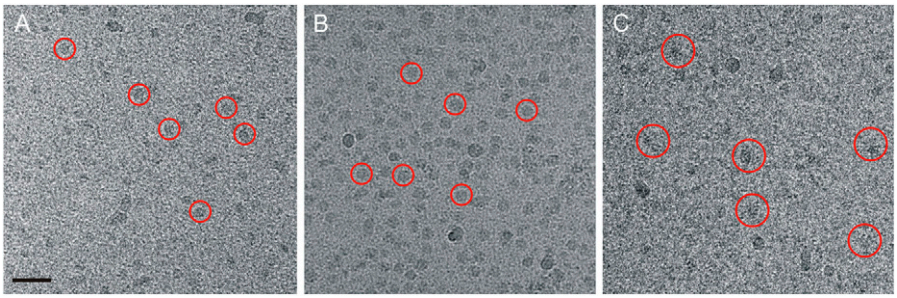

Fig. S1. Typical cryo-grids showing particles used for reconstructions. Sample particles are shown in red circles. (Scale bar, 35 nm.) (*A*) FcRY monomers at acidic pH. (*B*) FcRY dimers at acidic pH. (*C*) FcRY–IgY complexes.

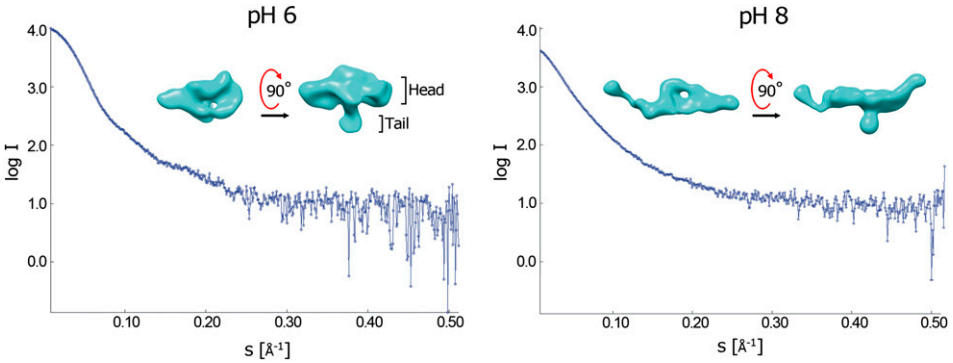

Fig. S2. SAXS analysis of FcRY at pH 6 and 8. Scattering intensities as a function of reciprocal Ångstroms for the FcRY monomer at pH 6 (*Left*) and pH 8 (*Right*). Examples of modeled structures fit to the SAXS data are shown for FcRY at pH 6 (*Left*) and pH 8 (*Right*).

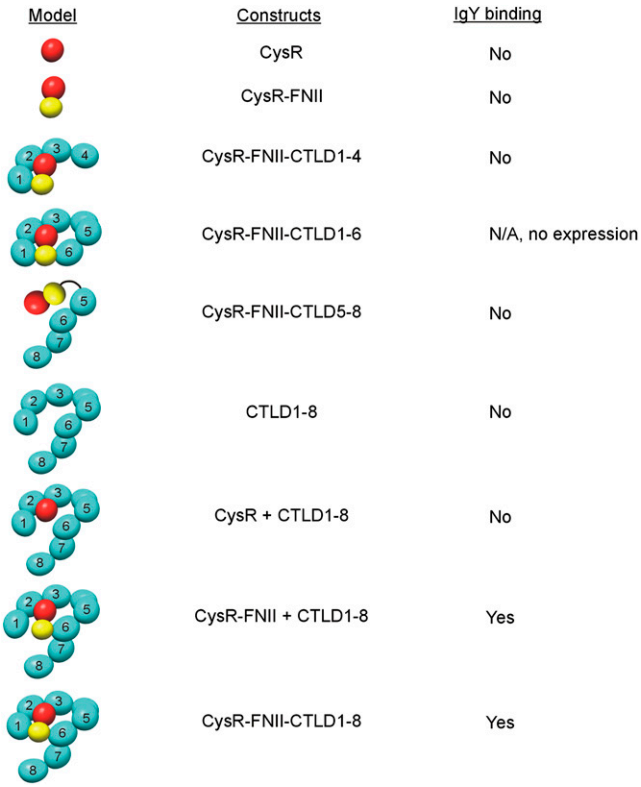

Fig. S3. Summary of FcRY truncation mutants and their IgY binding activities. Some of the results are taken from ref. 5. (*Left*) Schematic models of the domains in the FcRY mutants. (*Center*) FcRY constructs that were expressed and tested. (*Right*) Binding to IgY that was detectable using a surface plasmon resonance (SPR) binding assay (as described in ref. 5) is listed as "Yes."

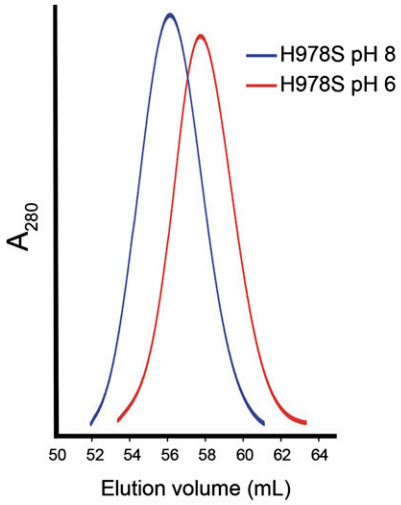

Elution volume (mL)	Wild-type	H159Y	H387Q	H538Q	H962Y	H978S
pH 6	57.9	58.2	57.6	58.3	57.9	57.7
pH 8	56.3	56.6	56.0	56.6	56.3	56.1
Shift	1.6	1.6	1.6	1.7	1.6	1.6

Fig. S4. pH-dependent conformational change in wild-type and mutant FcRY as assessed by size exclusion chromatography. (*Upper*) Example of size exclusion chromatography profiles at pH 6 and pH 8 for one of the FcRY mutants. Similar results were obtained for wild-type FcRY and the other FcRY histidine mutants. The faster migration at pH 8 than at pH 6 is consistent with a more elongated structure at basic pH than acidic pH, as also indicated by the SAXS analysis (Fig. S2). (*Lower*) Summary of elution conditions for mutant vs. wild-type FcRY at acidic and basic pH values.